Authors' comments to Anonymous Referee #2

We would like to thank the reviewer for the thorough review of our manuscript and insightful feedback. These comments have significantly improved the quality of our work. In the following sections, we present the reviewer's comments (in black), our responses (in red), and the changes made in the revised manuscript (in blue). Please note that all line numbers in our responses correspond to those in the revised manuscript.

Overall comments:

Review of "Latent heat feedbacks and the self-lofting of seeded ice plumes: Insights from bin microphysics simulations" by Zhang et al. 2026.

The article investigates the dynamical feedback associated with latent heat release from glaciogenic seeding of super-cooled stratus clouds using large-eddy simulations. A case from the CLOUDLAB field campaign is considered for this study. The authors found differences in the vertical spread of the seeded plume and its bulk microphysical properties depending on the dynamical condition at the time of seeding (updraft versus downdraft). Furthermore, the results revealed a reversal of the plume downdraft to an updraft at lower levels when seeding occurred during a downdraft. Building on these findings, the authors hypothesize that differences in plume properties are primarily driven by variations in latent heat release during depositional ice growth. To support this claim, they show accumulated latent heat and its relation to the difference in vertical velocity.

In my opinion, the manuscript is well written and will be a nice contribution to ACP. I only have the following minor comments and suggestions.

Specific comments:

1. Figure 6 – Please show separate plots from the simulations with updraft and downdraft seeding conditions. It will help visualize the evolution of the plume structure and be helpful for the readers to follow the later discussion. I also wonder if the detailed plume structure could be visualized a bit better (zooming over the plume location).

   Thanks for this suggestion. We have included 3D animations of the ice plume for the reference case, as well as for the 6 min (strongest initial updraft) and 10 min (strongest downdraft) simulations. The animations are presented either from a fixed viewing angle or from a camera following the ice plume. The corresponding

data links are provided in the Appendix. We believe that these 3D visualizations will help readers better understand the spatial structure of the ice plume.

L245-249:

The ice plume initially appears as a localized feature, with a horizontal extent of approximately 300 m and a top height near 400 m 4 min after INPs are released into the computational domain (Fig. 6; see also Appendix A for 3D visualizations of the ice plume from the model simulations).

2. L184: What's the third factor? The authors listed only two but mentioned: "attributed to three factors." I assume the ice nucleation could be another major contributor to the deviation. Is there any difference in ice nucleation magnitude and locations? Do you think a stochastic ice-nucleation scheme would yield more differences?

   Thanks. We agree that the deterministic nature of our current ice nucleation parameterization is indeed a major contributor to the reduced variability in the simulated results compared to observations. We have added the point into the main text.

   L234-235:

   ; and (3) the use of a deterministic ice nucleation scheme, which may underestimate the natural stochastic variability of ice initiation.

3. L213-217: It would be much clearer and more convincing if the authors showed the local buoyancy tendencies arising from latent heat release and condensate/ice loading. Such tendencies would be straightforward to analyze from the LES model output to confirm the hypothesis. Another option is to turn off the latent heating feedback in the ice plume to directly test the hypostasis.

   We fully agree with the reviewer's suggestion. To directly test our hypothesis and provide a clearer physical picture, we followed the reviewer's "second option" by conducting additional sensitivity simulations where the latent heating feedback was systematically manipulated. Specifically, we performed 40 additional ensemble simulations to decompose the thermodynamic drivers:

   - WBF-off seeding case ($L_s = L_c$): By setting the latent heat of sublimation equal to the latent heat of condensation, we effectively "turned off" the net latent heat gain ($L_f = L_s - L_c$) associated with the WBF process, while still retaining the initial heat from droplet freezing.
   - No-ice seeding case: This serves as a passive baseline without any microphysical–thermodynamic feedback.

   Furthermore, as suggested in the first part of the reviewer's comment, we have added buoyancy analysis (Figure 11) to the revised manuscript as detailed in the new Section 4.3 (L268–290).

L29-38:

Following the initial ice initiation—the so-called "latent heat kick" from droplet freezing—the ice phase undergoes rapid diffusional growth. During this stage, the latent heating produced by sublimation/deposition significantly outweighs the additional weight of the ice phase (condensate loading), effectively invigorating the cloud plume. While some studies have explored the resilience of cloud microphysics to environmental changes (Grabowski and Morrison, 2021), the specific roles of the initial freezing "kick" versus the subsequent feedbacks driven by the WBF mechanism and adiabatic cooling in governing plume dynamics remain under-examined. A fundamental question, therefore, arises: to what extent is the evolution of an ice plume determined by the initial vertical wind conditions at the time of nucleation, as opposed to being sustained and amplified by the seeding-induced microphysical–thermodynamic feedbacks—including both the initial latent heat 'kick' from droplet freezing and the subsequent latent heat release associated with the transition from liquid and vapor to the ice phase?

L190-204:

To further isolate the physical mechanisms driving the plume evolution and to address the relative importance of the initial latent heat "kick" versus the subsequent WBF-driven feedbacks, two additional sets of 20-member ensemble simulations were conducted. These 40 simulations use the same initiation times as the original seeding ensemble to ensure a direct comparison under identical dynamical backgrounds: (1) WBF-off seeding case ($L_s = L_c$): In these simulations, the latent heat of sublimation (L_s) is set equal to the latent heat of condensation (L_c) in the model's thermodynamic equations. This modification effectively eliminates the net latent heat gain ($L_f = L_s - L_c$) otherwise produced when ice crystals grow at the expense of cloud droplets (the WBF process). Furthermore, it ensures that any depositional growth driven by adiabatic cooling during the plume's ascent only releases heat equivalent to L_c, thereby removing the extra energetic contribution of freezing (L_f). This setup allows the initial latent heat release from the freezing of cloud droplets (the "initial kick") to occur normally while suppressing the enhanced thermodynamic feedback during subsequent ice growth; (2) No-ice seeding case: In this baseline ensemble, INPs are released into the domain as passive tracers, but the ice nucleation process is disabled. This case serves as a reference to represent the plume's evolution governed solely by the background turbulent flow, in the absence of any microphysical–thermodynamic feedbacks. By comparing these two sensitivity ensembles with the original seeding simulations, we can quantitatively

decompose the total buoyancy gain into contributions from the initial freezing event and the subsequent growth-driven intensification supported by both WBF and adiabatic cooling.

L297-334:

4.3 Decomposing thermodynamic drivers: delayed feedback and the role of WBF

To disentangle the distinct thermodynamic drivers of the plume evolution, we compare the ice plume trajectories and their corresponding mean buoyancy across three sensitivity configurations: the Normal, WBF-off, and no-ice seeding cases (Figs. 9 and 12). To provide a more quantitative assessment of the time evolution, we analyze the accumulated altitude differences between these configurations in 100-s intervals (Fig. 11). During the initial stage of evolution ($t < 300$ s), the trajectories remain nearly identical, which is physically explained by the evolution of plume buoyancy shown in Fig. 12. In the first 200 seconds, the buoyancy across all three ensembles shows minimal deviation and the accumulated height differences remain close to zero (Fig. 11). This indicate that neither the initial latent heat of freezing nor the WBF growth exerts a significant immediate influence on the plume's altitude. During this period, vertical motion is almost entirely governed by the pre-existing environmental vertical velocity.

A distinct thermodynamic response emerges as the plumes evolve. Between $t = 200$ s and $t = 500$ s, the buoyancy of both the Normal and WBF-off cases begins to increase significantly relative to the no-ice-nucleation baseline. As shown in Fig. 11, the height difference between the WBF-off and No-ice cases (green line) rises more rapidly than the difference between the Normal and WBF-off cases (blue line) during this interval. This suggests that the initial buoyancy gain is primarily attributed to the latent heat released during the freezing of cloud droplets and the onset of depositional growth at the condensation rate (L_c). This pulse of energy provides the impulse for the "secondary ascent" observed after 300 s.

The mature stage ($t > 600$ s) is characterized by a secondary divergence in buoyancy, where the Normal plumes (solid lines in Fig. 12) exhibit a consistently higher rate of buoyancy increase compared to the WBF-off ($L_s = L_c$) plumes (dashed lines). Also, the accumulated height difference between the Normal and WBF-off cases (blue line in Fig. 11) shows a steady, non-linear increase over time. These two divergences represent the combined thermodynamic

contribution of the WBF process and the enhanced depositional growth driven by adiabatic cooling. By extracting the latent heat of freezing (L_f) during the transition from both liquid and vapor phases to ice, these processes act as a persistent "internal engine" that sustains the plume's upward momentum.

This late-stage effect is quantified in Fig. 10 by calculating the ratio R_{WBF}:

$$R_{\mathrm{WBF}} = \frac{Z_{\mathrm{Normal}} - Z_{\mathrm{WBF\ off}}}{Z_{\mathrm{Normal}} - Z_{\mathrm{no\ ice}}}$$

The WBF-driven heating accounts for approximately 25% to 30% of the total seeding-induced altitude gain. While the freezing component accounts for the majority (70%) of the total thermodynamic invigoration, the buoyancy plots confirm the reviewer's intuition that the WBF growth is critical for sustaining the upward momentum in the mature stage of the plume's life cycle.

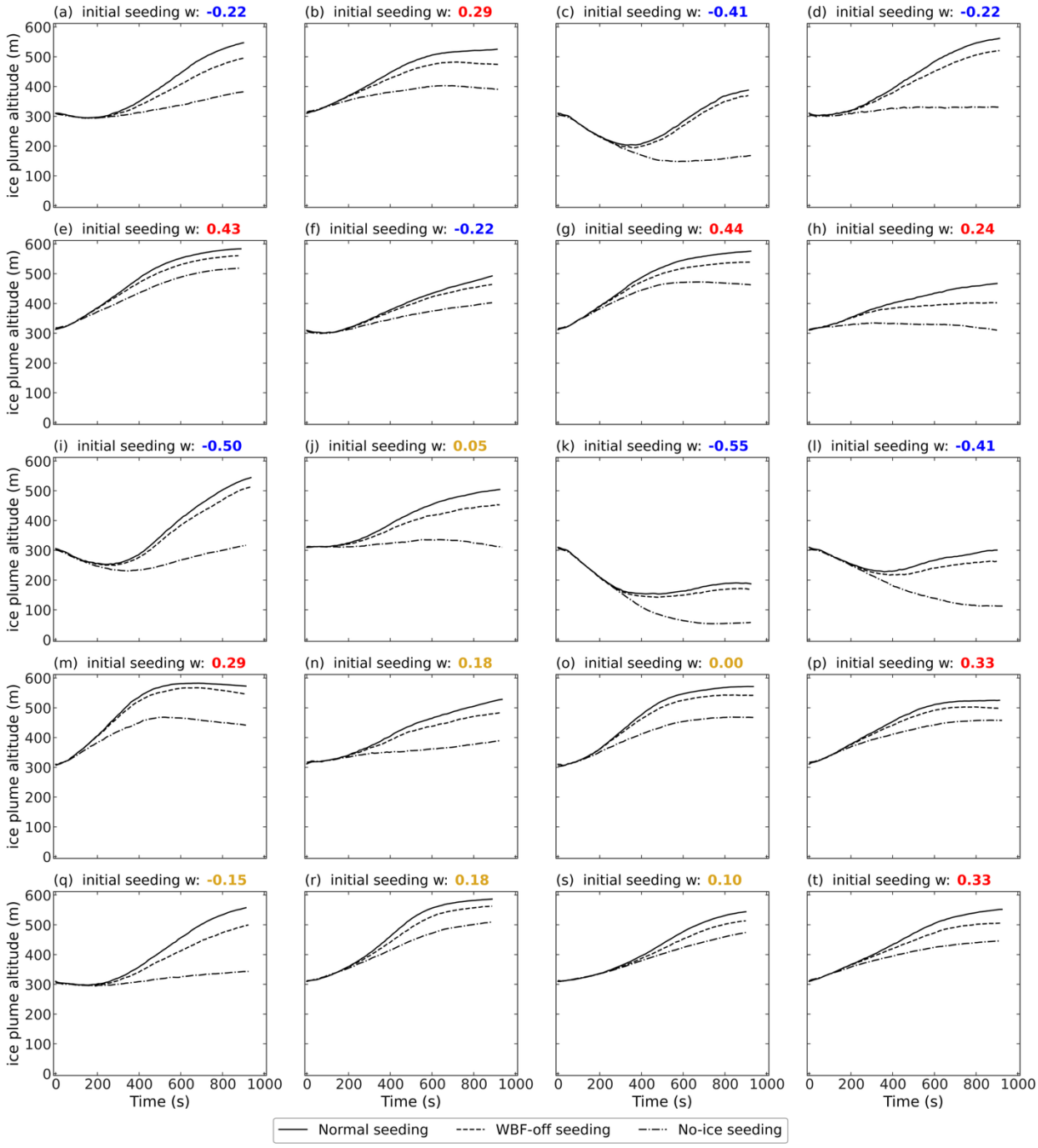

Figure 9 Time evolution of the mean altitude of the ice plume in all simulations, with INP injection initiated at 1-minute intervals from 0 to 1140 s (19 min). Solid curves represent the default configuration; dashed curves show results from simulations in which latent heating associated with the WBF process is disabled by setting the latent heat of sublimation equal to that of evaporation; dash-dotted curves indicate the mean altitude of INPs in simulations without ice nucleation

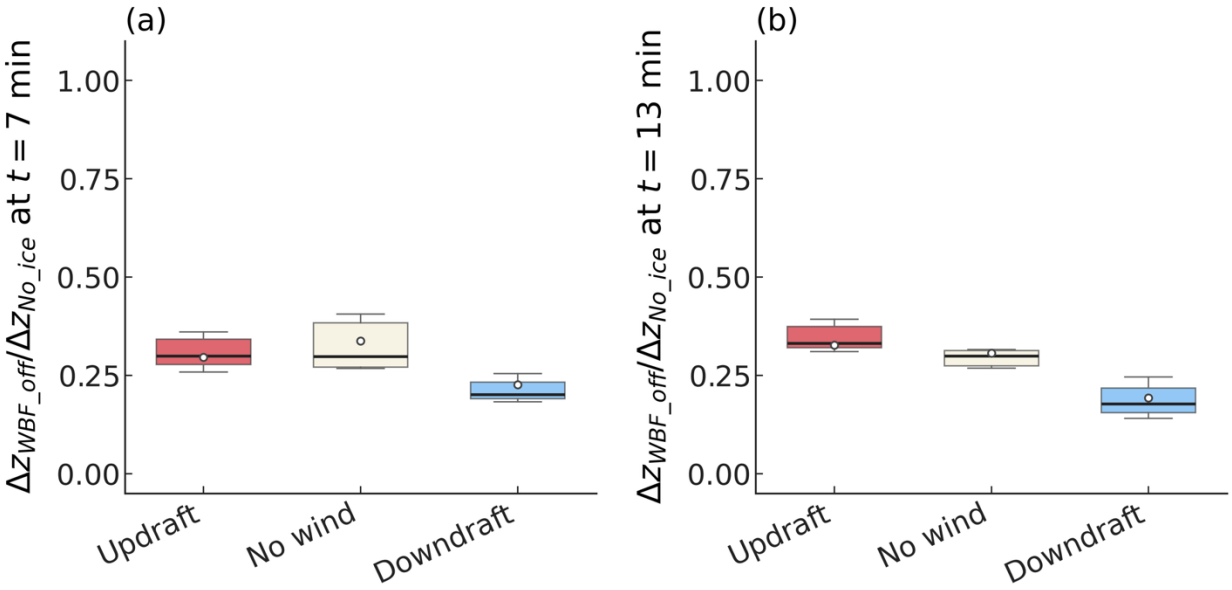

Figure 10 The ratio of the mean-altitude difference between the default and no-WBF-heating simulations to that between the default and no–ice-nucleation simulations at (a) 7 and (b) 13 min. Here, R_{WBF} is defined in eq. 2.

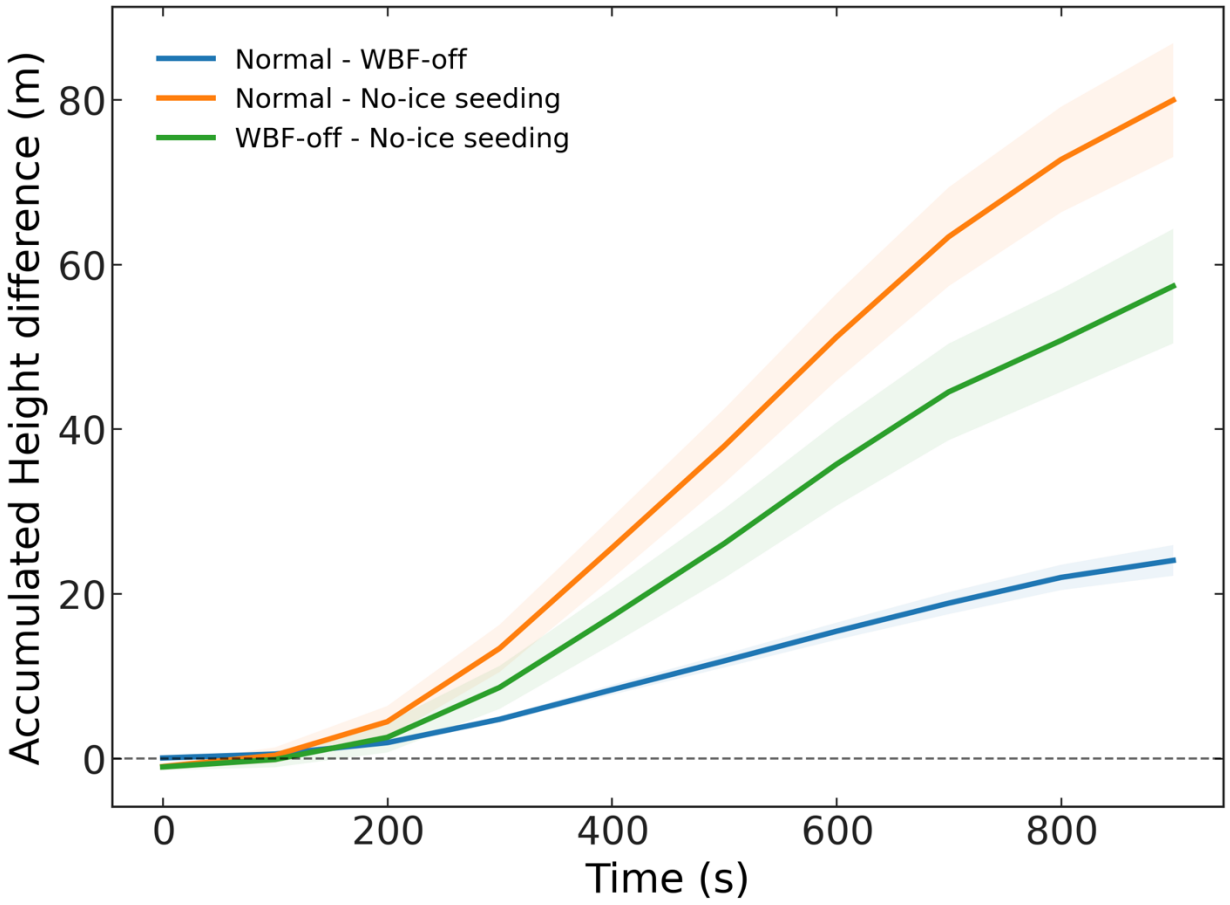

Figure 11 Time evolution of the accumulated plume-height differences between the three model configurations: Normal, WBF-off, and No-ice seeding. The height difference is calculated as the difference in mean plume altitude between two configurations within 100 s time intervals and averaged over all trajectories. Positive values indicate that the first configuration exhibits a higher plume altitude than the second configuration. Shaded regions represent the standard error of the mean across trajectories.

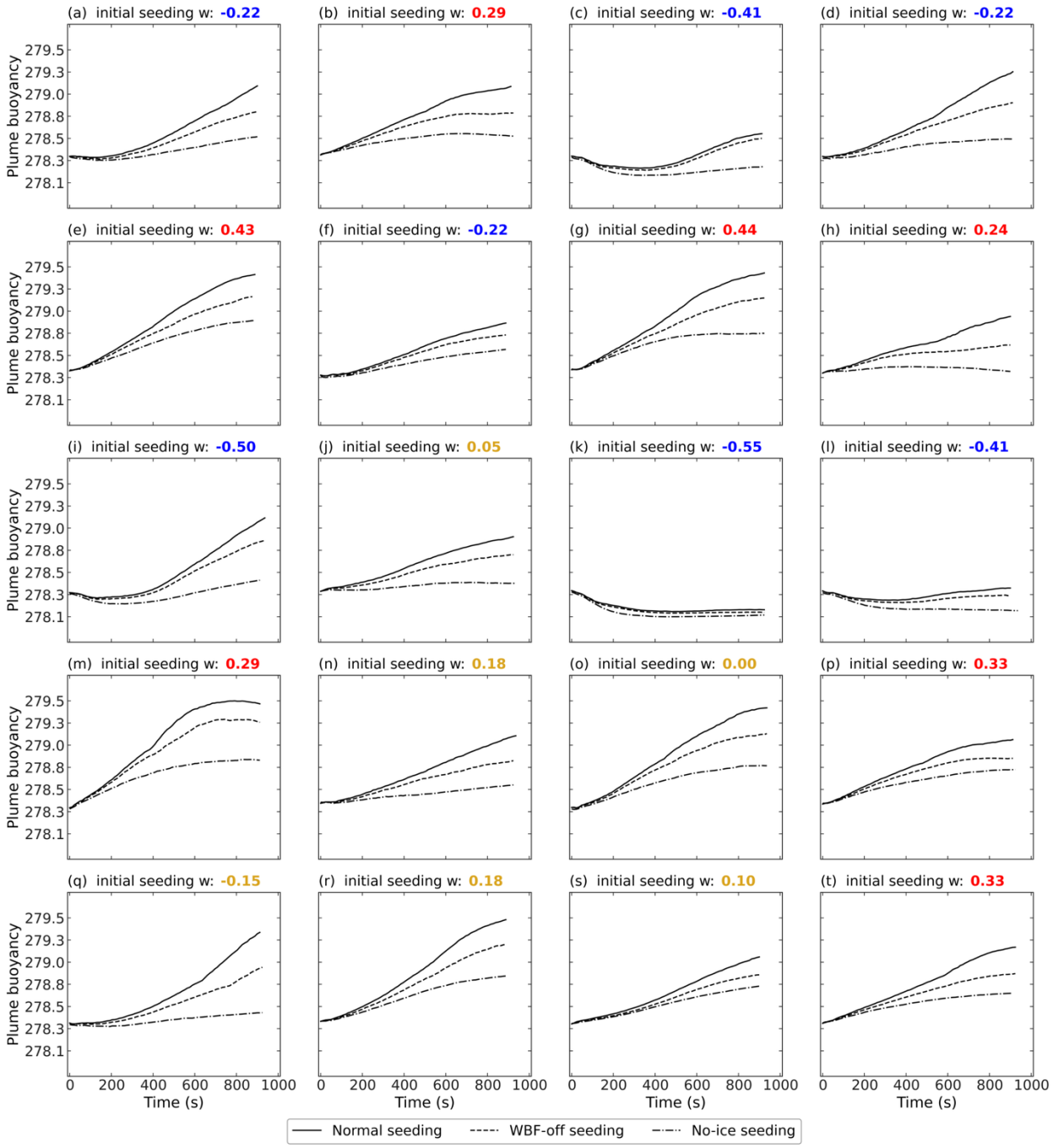

Figure 12 Same as Fig. 10, but for the time evolution of the mean buoyancy of the ice plume.

4. L221: What do you mean by 'accumulated heat' and \Delta W? Please define it clearly (how is it calculated?).
   We have added this explanation for accumulated latent heat to the text (Section 4.2).
   L271-275:

The cumulative latent heat is calculated as the time-integral of the net phase-change energy within the plume cells (defined as grid cells where ICNC exceeds the 70th percentile, corresponding to ICNC values of approximately 100 L^{-1} or greater). This term specifically represents the excess heating relative to the non-seeded baseline ($Q - Q_{\text{no ice}}$), thereby isolating the latent heat of freezing and the net heating from the WBF process while excluding the background latent heat of condensation associated with the ambient cloud.

5. L227: I can't see any appendix in the paper. Also, the appendix reference is missing ("see Appendix „„"). Did the authors remove it at some point? Please clarify or add the appendix figure.
   Added, thanks!
   L430-432:
   Appendix A: Three-dimensional animations
   Three-dimensional animations of the simulated ice and liquid mixing ratios, corresponding to INP injection initiated at 6 min (strongest updraft), 9 min (reference case), and 10 min (strongest downdraft), are available at https://zenodo.org/records/19731239.

6. Figure 9 – Would it be possible to plot the time evolution of the vertical profile instead of the mean values (could also be added as another supporting figure in the appendix)? Since vertical dispersion differs between the updraft and downdraft seeding, it will be interesting to see how the vertical profiles evolve.
   Added, thanks!
   L430-432:
   Appendix A: Three-dimensional animations
   Three-dimensional animations of the simulated ice and liquid mixing ratios, corresponding to INP injection initiated at 6 min (strongest updraft), 9 min (reference case), and 10 min (strongest downdraft), are available at https://zenodo.org/records/19731239.

7. L261-263: This is an interesting finding that PSDs are so resilient. It is a bit counterintuitive. I imagined that, with variabilities in nucleation altitude (and difference in vertical dispersion rates) between the downdraft- and updraft-seeded plumes, the PSD evolution (especially size dispersion) would differ due to different growth/supersaturation exposure histories. I wonder whether the finding is consistent across local PSDs constructed at different altitudes over time.
   We agree with the reviewer that the resilience of the PSD shape is an intriguing finding. We have added more discussion to the revised manuscript.

L351-368:

The evolution of the size distribution of the ice crystals confirms that while the growth rate varies, the growth mode remains consistent. Figure 14 displays the PSD at downstream distances of y = 2, 3, and 4 km. Across all wind conditions, the PSDs exhibit a coherent rightward shift (towards larger diameters) over time. The PSD in the downdraft regime exhibits a broader (i.e., flatter) shape than in the other two regimes. This can be attributed to the larger vertical extent of the ice plume, which exposes ice particles to varying temperatures and, consequently, different diffusional growth rates at different altitudes. In addition, the initial downward trajectory exposes the ice particles to an environment with lower ice supersaturation, and part of the ice plume even descends below the cloud layer (see Appendix A). As a result, the number concentration of small particles (diameter < 200 μm) remains relatively high, even after the ice plume has traveled 4 km.

The structural similarity of the PSDs in the no-wind and updraft regimes suggests that the seeding mechanism primarily determines the initial spectral characteristics, whereas the environmental updraft velocity mainly modulates the rate of spectral shift rather than altering the fundamental shape of the distribution. This is likely because, in both regimes, the ice plume follows a similar trajectory toward the cloud top, with the key difference being that the onset of upward motion occurs earlier in the updraft regime.

The PSDs across the three regimes become increasingly similar at the same altitude in the simulations as the altitude increases (Fig. 15). This relative resilience of the PSD shape likely stems from the horizontally homogeneous quasi-uniform supersaturation environment within the liquid-dominated cloud layer, where ice crystals grow under similar vapor pressure deficits relative to water saturation regardless of their vertical trajectory. Furthermore, sedimentation does not yet play a significant role.

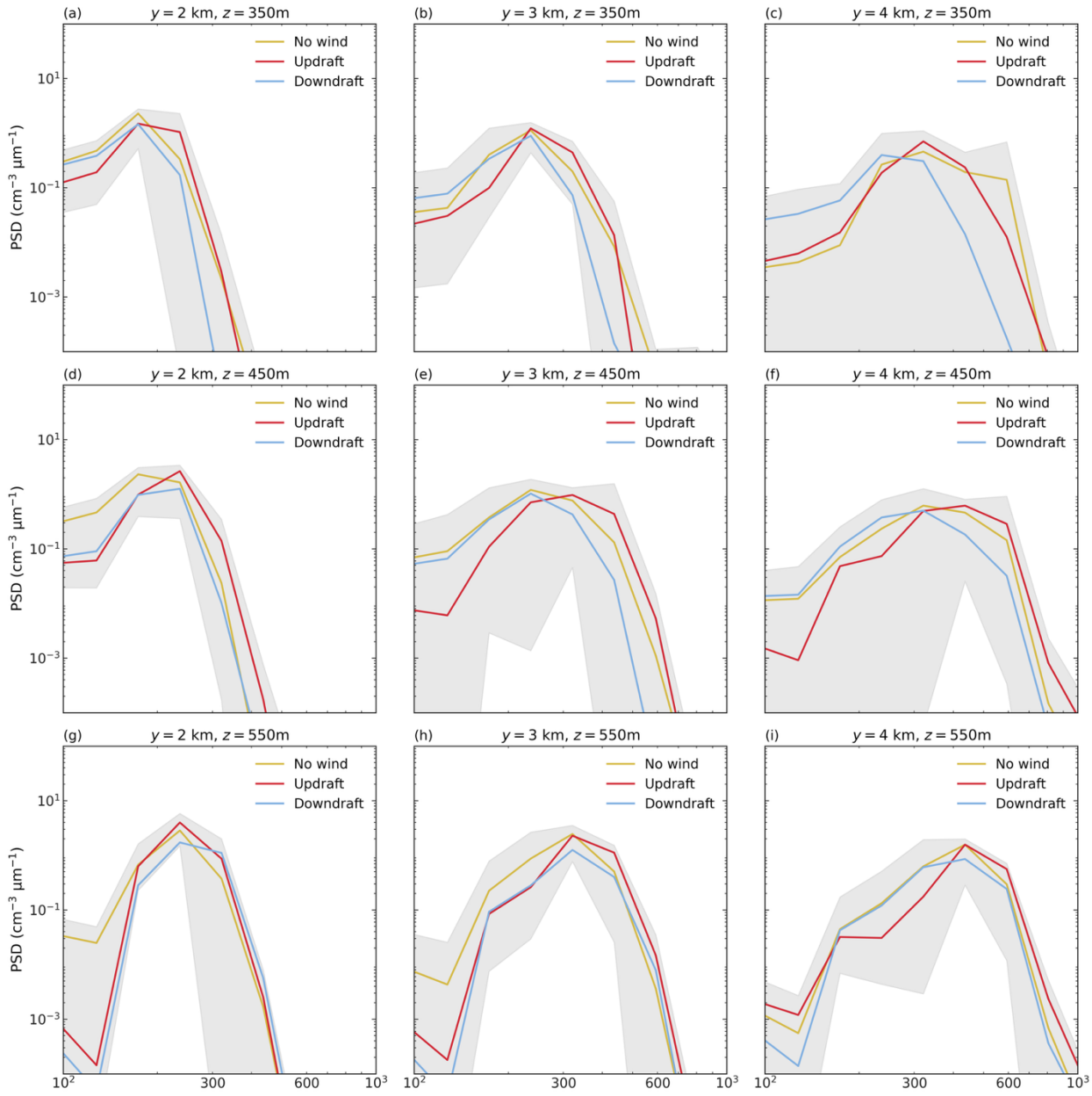

Figure 15 Same as Fig. 14, except that the PSD is shown at fixed altitudes of 350 m (a–c), 450 m (d–f), and 550 m (g–i).